Supporting Information

Shackman et al. 10.1073/pnas.1214364110

SI Methods

Hypothesis testing used the sample described in ref. 1, which focused on the heritability of metabolic activity in the medial temporal lobe. Methods for the elicitation and assessment of anxious temperament (AT) and the quantification of ^{18}fluorodeoxyglucose (FDG)-positron emission tomography (PET) are detailed in refs 1 and 2 and summarized here.

Subjects. Briefly, 240 prepubescent monkeys [*Macaca mulatta*; mean (SD) age = 2.41 (0.92) years; 51.3% female] from the Harlow Primate Laboratory or Wisconsin National Primate Research Center underwent behavioral testing and FDG-PET as part of a larger investigation of the genetic underpinnings of AT (1, 3). PET data from two individuals proved unusable. Housing and experimental procedures were performed in accord with guidelines set forth by the University of Wisconsin–Madison Institutional Animal Care and Use Committee.

Overview. Subjects received intravenous FDG immediately before the 30-min No-Eye Contact (NEC) challenge. Individual differences in behavioral responses (freezing and vocalizations) were quantified by an experienced observer. Following testing, plasma was collected for quantifying cortisol and subjects were deeply anesthetized (15 mg/kg ketamine), intubated, and positioned in a stereotactic device within the PET scanner. Metabolic activity during the PET scan reflects the amount of FDG uptake during the preceding behavioral paradigm; regions that were more metabolically active during the NEC challenge took up more radio-labeled glucose. Anesthesia was maintained using 1–2% (vol/vol) isoflurane gas. MRI were collected during a separate session. The median (SD) time between the FDG-PET and MRI sessions was 37.0 (37.5) d.

NEC Challenge. Individual differences in the three dimensions of the AT phenotype were elicited using the NEC component of the Human Intruder Paradigm (HIP) (4). The HIP is among the most commonly used procedures for measuring dispositional anxiety in nonhuman primates (5). Subjects were placed in a testing cage. Similar to laboratory procedures used for assessing AT in children (e.g., stranger approach) (6–8), potential threat took the form of a male human experimenter ("intruder") who entered the room and stood motionless ~2.5 m while presenting his profile to the subject (30 min).

Quantifying Individual Differences in the Three Dimensions of the AT Phenotype. NEC-elicited behavior was unobtrusively quantified by a well-trained rater using a closed-circuit audiovisual system. Freezing was defined as a period of >3 s characterized by a tense body posture and the absence of vocalizations or movements other than slow head movements or eye-blinks. "Coo" calls are contact or separation vocalizations that are elicited by exposure to the test cage (i.e., the "alone" condition of the HIP) and suppressed by exposure to the NEC challenge (i.e., human intruder's profile) (9–11). Coo vocalizations were defined as audible calls characterized by an increase then decrease in frequency and intensity made by rounding and pursing the lips. Mean freezing duration and cooing frequency were $\log_e$ and square-root transformed, respectively. Plasma cortisol (μg/dL) was quantified in duplicate using the DPC Coat-a-count radioimmunoassay (Siemens). Assaying procedures were highly reliable (interassay CV = 6.6%; intra-assay CV = 4.0%) and sensitive (lower detection limit = 1 μg/dL). Standardized cortisol, freezing, and vocalization responses were created (1, 2) by linearly removing nuisance variance in age and, for cortisol, time-of-day using SPSS (v20.0.0; IBM). Prior work indicates that cortisol, freezing, and coo vocalizations consistently show robust changes in response to the NEC challenge (4, 5, 11–23). Brain-behavior analyses used reverse-scored vocalizations ("vocal reduction" = $-1 \times \text{coo-frequency}^{1/2}$) to ensure that effects were consistently signed across the three dimensions of the phenotype (i.e., higher values indicate more intense reactions to the phenotype-eliciting NEC challenge).

FDG-PET and MRI. FDG and attenuation scans were acquired using a Siemens/Concorde microPET P4 scanner (24). Images were reconstructed using standard filtered-backprojection techniques with attenuation- and scatter-correction. MRI were collected under anesthesia (see above) using a General Electric Discovery 3T scanner (GE) and standard quadrature extremity coil. Scans used a 3D T1-weighted inversion-recovery fast gradient echo prescription (TR/TE/Flip/ NEX /FOV/Matrix: 9.4 ms/2.1 ms/10°/2/140 mm/512 × 512; 248 × 1-mm axial slices; gap: –0.05 mm).

Processing Pipeline for Imaging Data. Before spatial normalization, brains were manually extracted from T1 images using SPAMALIZE (http://psyphz.psych.wisc.edu/~oakes/spam/spam_frames.htm). Brain-extracted T1 images were linearly registered (12 *df*) to a preexisting in-house macaque template (2) in the stereotactic space of Paxinos et al. (25) using FLIRT (http://fsl.fmrib.ox.ac.uk/fsl/flirt). Images were inspected and averaged to create an age-appropriate, study-specific linear template (0.625 mm × 0.625 mm × 0.625 mm = 0.244 mm^3). Native-space, brain-extracted T1 images were then nonlinearly registered to the template using FNIRT (http://www.fmrib.ox.ac.uk/fsl/fnirt). Normalized brains were segmented into gray matter (GM), white matter, and cerebrospinal fluid probability maps using FAST (www.fmrib.ox.ac.uk/fsl/fast4). Single-subject PET images were linearly registered to the corresponding native-space T1 images (6 *df*). The resulting transformation matrices were concatenated with those defining the nonlinear transformation to the study-specific standard template and then used to normalize the PET images. Normalized and interpolated PET images (0.625 mm × 0.625 mm × 0.625 mm = 0.244 mm^3) were global-mean scaled within the brain using SPAMALIZE. Scaled PET and GM probability maps were spatially smoothed (4-mm FWHM Gaussian). Some figures were created using MRIcron (http://www.mccauslandcenter.sc.edu/mricro/mricron).

Hypothesis Testing Strategy. The central aim of the present study was to distinguish common and selective neural substrates. Accordingly, we first identified regions where metabolic activity predicted variance in each of the three dimensions of the AT phenotype (cortisol, freezing, and vocal reduction) while controlling for the other two. Specifically, a series of whole-brain robust regression analyses were performed using MULTISTATIC (26), an extension of FMRISTAT (http://www.math.mcgill.ca/keith/fmristat). Consistent with recent recommendations (27, 28), analyses used robust procedures, which minimize the influence of outlying observations. Similar to other toolboxes for imaging data (29), robust regression in MULTISTATIC is implemented using the *robustfit* function in MATLAB (http://www.mathworks.com). In each analysis, one of the dimensions served as the explanatory variable and the other two served as covariates of no interest. Analyses also controlled for nuisance variation in mean-centered age, sex, and voxelwise GM probability, an indirect measure of differences in spatial normalization and gross anatomy (26). This analytic procedure is formally equivalent to computing three voxelwise partial correlation maps.

Common substrates. Common neural substrates are those shared by individuals with varying expressions of extreme AT, a core set of brain regions where metabolism predicts variation in all three AT dimensions (cortisol levels, freezing behavior, and vocal reductions). To identify regions where individual differences in regional brain metabolism significantly predicted all three AT dimensions, the three partial correlation maps were thresholded using the false-discovery rate (FDR $q = 0.05$; whole-brain corrected across maps) (30, 31) and then combined using a three-way minimum conjunction test (i.e., logical AND) (32). The conjunction test yielded a "*t*-minimum" map containing voxels that were significant in all three parent maps; voxels satisfying this criterion were assigned the value corresponding to the *t*-statistic from the least-significant parent map, otherwise set to 0 (www.math.mcgill.ca/keith/fmristat/#conjunctions).

Selective substrates. Selective neural substrates are those specifically engaged by individuals with high levels of a particular dimension of the AT phenotype (e.g., freezing), regions where metabolism significantly and strongly predicts variation in only one of the AT dimensions. Selective regions were defined as those that: (*i*) were significantly correlated with one of the three dimensions of the AT phenotype (cortisol levels, freezing behavior, or vocal reductions; FDR $q < 0.05$), and (*ii*) explained significantly more variance in that dimension compared with the other two (FDR $q < 0.05$). Effectively, this process identified partial correlations that were both significant and significantly different from the other two (e.g., individual differences in freezing explained more variance in brain metabolic activity than cortisol and vocal reductions). Differences in correlations correlations were assessed using the Hotelling–Williams test (33, 34).

Mediation analyses. We identified the lateral division of the central nucleus of the amygdale (CeL) and anterior hippocampus as common substrates, regions where metabolism predicts each one of three dimensions constituting the AT phenotype (Fig. 3 and Table S4). To assess whether those brain-phenotype relationships are explained by activity in regions identified as selective, we used a series of multivariate mediation models to test whether the partial correlation between the common substrates and a particular dimension of the phenotype depends on the relevant selective substrate (e.g., CeL → M1 → freezing) (Fig. 4 and Tables S1–S3). We used a standard ordinary least squares (OLS) multivariate analytic framework (35, 36) (for recent applications to neuroimaging data, see refs. 37 and 38). Fully satisfying the criteria of this framework would demonstrate that a significant proportion of the association (i.e., partial correlation) between metabolic activity in one of the three common regions (e.g., CeL) and a particular AT dimension (e.g., freezing behavior) is predicted by metabolism in one of the candidate mediating region (e.g., M1, or the primary motor cortex). Operationally, this framework required four significant tests: (*i*) a common substrate predicts a particular dimension of AT, (*ii*) a selective substrate predicts a particular dimension of AT, (*iii*) the common substrate predicts the selective substrate, and (*iv*) controlling for variance in the selective substrate weakens the partial correlation between the common substrate and the relevant dimension of the AT phenotype. Consistent with our prior work (39), the final criterion was assessed using Clogg's test (35, 40). This test was conservatively thresholded at a nominal $P < 0.0057$ (Sidak-corrected for the nine tests-of-interest, one-tailed given the directional hypothesis). Because FDG-PET lacks the temporal resolution necessary to determine whether activity within the common substrates (e.g., CeL) temporally precedes differences in activity within the selective substrates (e.g., M1), this test does not provide evidence of causal mediation.

To assess the specificity of the mediation findings, we computed two kinds of control models (Table S5). For the first model, we recomputed each mediation model using another candidate mediator region as a control (e.g., using the cortisol-selective region for the freezing mediation model: CeL → lateral anterior hippocampus → freezing). For the second model, we recomputed each model using another AT dimension as a control (e.g., cortisol for the mediation model incorporating the freezing-selective region: CeL → M1 → cortisol). Control analyses were only computed for regions where significant mediation effects were obtained.

Phenotype Reliability Analyses. We computed test-retest reliability of individual differences in cortisol, freezing behavior, and vocal reductions for a subset of individuals exposed to the NEC challenge on three occasions over 1.21 y (SD = 0.27; $n = 63$). The first assessment occurred at the time of FDG-PET session featured in the main text. The rank-order of individual differences in cortisol, freezing, and vocal reduction were reliable over the three occasions (intraclass correlation = 0.66–0.88; mean single-response correlation between adjacent sessions = 0.46–0.79). These levels are similar to those obtained for self-report measures of affective traits (e.g., negative affect) in human adults over comparable spans (41). The true psychometric reliability of these measures (i.e., in the absence of genuine change) is likely to be somewhat higher because of the lengthy period from the first to the third sessions (42) and the fact that data were acquired during the peri-adolescent period, a period of substantial neural and psychological maturation (43). The composite index of AT (2) was also reliable (intraclass correlation = 0.83; mean correlation between adjacent sessions = 0.71).

Hemispheric Asymmetry Analyses for the Right Dorsal Amygdala. To test whether the right dorsal amygdala cluster identified by the three-way voxelwise conjunction (see Fig. 3 and Table S4) showed a significant hemispheric asymmetry, we computed the difference in correlations separately for each dimension of the AT phenotype. Regressions were conducted in SPSS using data extracted from the right dorsal amygdala cluster and the homologous region in the left hemisphere, and controlling for nuisance variance in mean-centered age, sex, and GM probability. Because none of the tests approached significance, $t < 1.46$, $P > 0.14$ (uncorrected), we refrain from interpreting the apparent laterality of this effect.

Probabilistic Chemoarchitectonic Map of the CeL. The amygdala is a complex structure, comprised of numerous anatomically and physiologically distinct nuclei (44). Here we used previously published in vivo serotonin transporter (5-HTT) binding data (45, 46) to localize the dorsal amygdala cluster to the CeL of the amygdala. Ex vivo research demonstrates that the lateral division of the primate central nucleus of the amygdala (CeL) expresses much higher 5-HTT levels compared with neighboring regions (47–50). Capitalizing on this chemoarchitectonic signature, we used the distribution of ^{11}C-DASB (a high-affinity radiolabeled 5-HTT ligand) from an independent sample of young monkeys to define a probabilistic CeL region of interest (Fig. S1). For detailed methods, see ref. 45; for a similar mapping application, see ref. 51. Briefly, 5-HTT availability was assayed using ^{11}C-DASB, a radiolabeled high-affinity 5-HTT ligand. Dynamic PET time series were transformed into voxelwise distribution volume ratio [DVR; an index of binding (52)] maps normalized to activity in a cerebellar reference region. Single-subject DVR maps were normalized to the study-specific template and averaged. The resulting probabilistic (i.e., mean) 5-HTT binding map was thresholded (250× cerebellum). We then assessed the degree of overlap with the conjunction-defined cluster. This process revealed that the peak amygdala voxel and most of the dorsal amygdala cluster overlapped with the ROI (Sørensen-Dice similarity coefficient = 0.86), indicating that individuals with different presentations of extreme AT commonly engage the CeL (Fig. S1).

AT Composite Is a More Sensitive Index of Metabolic Activity than any One of Its Constituents. The results of the conjunction analysis suggest, but do not demonstrate, that aggregating the three dimensions—cortisol, freezing, and reduced vocalizations—into a composite would provide a more sensitive index of AT-related variation in core network activity. Confirmatory analyses demonstrated that this was the case. Confirmatory analyses used techniques similar to those described in *Hypothesis Testing Strategy* (see above), but did not partial covariation across the three dimensions. This process revealed that the AT composite, computed as the arithmetic mean of the three standardized dimensions (2), explained significantly more variance in CeL and anterior hippocampal metabolic activity than any one of the constituent dimensions in the clusters identified by the voxelwise three-way conjunction analysis, $t > 2.18$, $P < 0.03$. Furthermore, planned contrasts revealed that the slope of the robust regression line fit to neural activity was significantly steeper for the AT composite compared with its constituents ($P < 0.04$, one-tailed). This finding indicates that individuals with a strong average response to the NEC—high levels of cortisol, long bouts of freezing, and few vocalizations—tended to show the highest levels of activity in the CeL and anterior hippocampus; conversely, individuals with a weak average response tended to show the lowest activity. Whole-brain analyses yielded similar conclusions.

These results also provide unique empirical support for the use of composite measures of AT and other dimensions of temperament. Often, such composites are derived using statistical criteria that mandate strong covariation among constituents (e.g., factor analysis). Our results empirically demonstrate the utility of multidimensional composites constructed from anxiety-related measures that are theoretically or clinically related, but not necessarily significantly intercorrelated. In fact, our composite AT index showed strong predictive validity despite showing relatively weak covariation among its constituent dimensions, consistent with empirical work by Kagan et al. and others (7, 53–55).

1. Oler JA, et al. (2010) Amygdalar and hippocampal substrates of anxious temperament differ in their heritability. *Nature* 466(7308):864–868.
2. Fox AS, Shelton SE, Oakes TR, Davidson RJ, Kalin NH (2008) Trait-like brain activity during adolescence predicts anxious temperament in primates. *PLoS ONE* 3(7):e2570.
3. Rogers J, Shelton SE, Shelledy W, Garcia R, Kalin NH (2008) Genetic influences on behavioral inhibition and anxiety in juvenile rhesus macaques. *Genes Brain Behav* 7(4):463–469.
4. Kalin NH, Shelton SE (1989) Defensive behaviors in infant rhesus monkeys: Environmental cues and neurochemical regulation. *Science* 243(4899):1718–1721.
5. Corcoran CA, et al. (2012) Long-term effects of differential early rearing in rhesus macaques: Behavioral reactivity in adulthood. *Dev Psychobiol* 54(5):546–555.
6. Volbrecht MM, Goldsmith HH (2010) Early temperamental and family predictors of shyness and anxiety. *Dev Psychol* 46(5):1192–1205.
7. Kagan J, Reznick JS, Snidman N (1988) Biological bases of childhood shyness. *Science* 240(4849):167–171.
8. Hirshfeld-Becker DR, et al. (2008) Behavioral inhibition. *Depress Anxiety* 25(4): 357–367.
9. Fox AS, et al. (2005) Calling for help is independently modulated by brain systems underlying goal-directed behavior and threat perception. *Proc Natl Acad Sci USA* 102(11):4176–4179.
10. Bauers KA, de Waal FBM (1991) "Coo" vocalizations in stumptailed macaques: A controlled functional analysis. *Behaviour* 119(1–2):143–160.
11. Kalin NH, Shelton SE (1998) Ontogeny and stability of separation and threat-induced defensive behaviors in rhesus monkeys during the first year of life. *Am J Primatol* 44(2):125–135.
12. Kalin NH, Shelton SE, Davidson RJ, Kelley AE (2001) The primate amygdala mediates acute fear but not the behavioral and physiological components of anxious temperament. *J Neurosci* 21(6):2067–2074.
13. Izquierdo A, Murray EA (2004) Combined unilateral lesions of the amygdala and orbital prefrontal cortex impair affective processing in rhesus monkeys. *J Neurophysiol* 91(5): 2023–2039.
14. Izquierdo A, Suda RK, Murray EA (2005) Comparison of the effects of bilateral orbital prefrontal cortex lesions and amygdala lesions on emotional responses in rhesus monkeys. *J Neurosci* 25(37):8534–8542.
15. Machado CJ, Bachevalier J (2008) Behavioral and hormonal reactivity to threat: Effects of selective amygdala, hippocampal or orbital frontal lesions in monkeys. *Psychoneuroendocrinology* 33(7):926–941.
16. Golub MS, Hogrefe CE, Widaman KF, Capitanio JP (2009) Iron deficiency anemia and affective response in rhesus monkey infants. *Dev Psychobiol* 51(1):47–59.
17. Friedman EM, Reyes TM, Coe CL (1996) Context-dependent behavioral effects of interleukin-1 in the rhesus monkey (*Macaca mulatta*). *Psychoneuroendocrinology* 21(5):455–468.
18. Kalin NH, Shelton SE, Turner JG (1991) Effects of alprazolam on fear-related behavioral, hormonal, and catecholamine responses in infant rhesus monkeys. *Life Sci* 49(26):2031–2044.
19. Kalin NH, Shelton SE, Takahashi LK (1991) Defensive behaviors in infant rhesus monkeys: Ontogeny and context-dependent selective expression. *Child Dev* 62(5): 1175–1183.
20. Kalin NH, Shelton SE, Rickman M, Davidson RJ (1998) Individual differences in freezing and cortisol in infant and mother rhesus monkeys. *Behav Neurosci* 112(1):251–254.
21. Kalin NH, Larson C, Shelton SE, Davidson RJ (1998) Asymmetric frontal brain activity, cortisol, and behavior associated with fearful temperament in rhesus monkeys. *Behav Neurosci* 112(2):286–292.
22. Kalin NH, Shelton SE, Fox AS, Oakes TR, Davidson RJ (2005) Brain regions associated with the expression and contextual regulation of anxiety in primates. *Biol Psychiatry* 58(10):796–804.
23. Coleman K, Dahl RE, Ryan ND, Cameron JL (2003) Growth hormone response to growth hormone-releasing hormone and clonidine in young monkeys: Correlation with behavioral characteristics. *J Child Adolesc Psychopharmacol* 13(3):227–241.
24. Tai C, et al. (2001) Performance evaluation of the microPET P4: A PET system dedicated to animal imaging. *Phys Med Biol* 46(7):1845–1862.
25. Paxinos G, Huang X, Petrides M, Toga A (2009) *The Rhesus Monkey Brain in Stereotaxic Coordinates* (Academic, San Diego), 2nd Ed.
26. Oakes TR, et al. (2007) Integrating VBM into the General Linear Model with voxelwise anatomical covariates. *Neuroimage* 34(2):500–508.
27. Poldrack RA (2012) The future of fMRI in cognitive neuroscience. *Neuroimage* 62(20): 1216–1220.
28. Schwarzkopf DS, De Haas B, Rees G (2012) Better ways to improve standards in brain-behavior correlation analysis. *Front Hum Neurosci* 6:200.
29. Wager TD, Keller MC, Lacey SC, Jonides J (2005) Increased sensitivity in neuroimaging analyses using robust regression. *Neuroimage* 26(1):99–113.
30. Genovese CR, Lazar NA, Nichols T (2002) Thresholding of statistical maps in functional neuroimaging using the false discovery rate. *Neuroimage* 15(4):870–878.
31. Nichols T (2007) False discovery rate procedures. *Statistical Parametric Mapping. The Analysis of Functional Brain Images*, eds Friston K, Ashburner J, Kiebel S, Nichols T, Penny W (Elsevier, NY), pp 246–252.
32. Nichols T, Brett M, Andersson J, Wager T, Poline JB (2005) Valid conjunction inference with the minimum statistic. *Neuroimage* 25(3):653–660.
33. Steiger JH (1980) Tests for comparing elements of a correlation matrix. *Psychol Bull* 87(2):245–251.
34. Williams EJ (1959) The comparison of regression variables. *J R Stat Soc, B* 21(2): 396–399.
35. MacKinnon DP, Lockwood CM, Hoffman JM, West SG, Sheets V (2002) A comparison of methods to test mediation and other intervening variable effects. *Psychol Methods* 7(1):83–104.
36. Baron RM, Kenny DA (1986) The moderator-mediator variable distinction in social psychological research: Conceptual, strategic, and statistical considerations. *J Pers Soc Psychol* 51(6):1173–1182.
37. Lim SL, Padmala S, Pessoa L (2009) Segregating the significant from the mundane on a moment-to-moment basis via direct and indirect amygdala contributions. *Proc Natl Acad Sci USA* 106(39):16841–16846.
38. Wager TD, Davidson ML, Hughes BL, Lindquist MA, Ochsner KN (2008) Prefrontal-subcortical pathways mediating successful emotion regulation. *Neuron* 59(6):1037–1050.
39. Shackman JE, Shackman AJ, Pollak SD (2007) Physical abuse amplifies attention to threat and increases anxiety in children. *Emotion* 7(4):838–852.
40. Clogg CC, Petkova E, Shihadeh ES (1992) Statistical methods for analyzing collapsibility in regression models. *J Educ Stat* 17(1):51–74.
41. Watson D, Walker LM (1996) The long-term stability and predictive validity of trait measures of affect. *J Pers Soc Psychol* 70(3):567–577.
42. Chmielewski M, Watson D (2009) What is being assessed and why it matters: The impact of transient error on trait research. *J Pers Soc Psychol* 97(1):186–202.
43. Kalin NH, Shelton S (2000) The regulation of defensive behaviors in rhesus monkeys. *Anxiety, Depression, and Emotion*, ed Davidson RJ (Oxford Univ Press, NY), pp 50–68.
44. Freese JL, Amaral DG (2009) Neuroanatomy of the primate amygdala. *The Human Amygdala*, eds Whalen PJ, Phelps EA (Guilford, NY), pp 3–42.
45. Christian BT, et al. (2009) Serotonin transporter binding and genotype in the nonhuman primate brain using [C-11]DASB PET. *Neuroimage* 47(4):1230–1236.
46. Oler JA, et al. (2012) Evidence for coordinated functional activity within the extended amygdala of non-human and human primates. *Neuroimage* 61(4):1059–1066.
47. O'Rourke H, Fudge JL (2006) Distribution of serotonin transporter labeled fibers in amygdaloid subregions: implications for mood disorders. *Biol Psychiatry* 60(5): 479–490. Available at www.sciencedirect.com/science/journal/00063223.
48. Freedman LJ, Shi C (2001) Monoaminergic innervation of the macaque extended amygdala. *Neuroscience* 104(4):1067–1084.
49. Bauman MD, Amaral DG (2005) The distribution of serotonergic fibers in the macaque monkey amygdala: An immunohistochemical study using antisera to 5-hydroxytryptamine. *Neuroscience* 136(1):193–203.

50. Yilmazer-Hanke DM (2012) Amygdala. *The Human Nervous System*, eds Mai JK, Paxinos G (Academic, San Diego), pp 759–834.
51. Oler JA, et al. (2009) Serotonin transporter availability in the amygdala and bed nucleus of the stria terminalis predicts anxious temperament and brain glucose metabolic activity. *J Neurosci* 29(32):9961–9966.
52. Innis RB, et al. (2007) Consensus nomenclature for in vivo imaging of reversibly binding radioligands. *J Cereb Blood Flow Metab* 27(9):1533–1539.
53. Kagan J, Snidman N, McManis M, Woodward S, Hardway C (2002) One measure, one meaning: multiple measures, clearer meaning. *Dev Psychopathol* 14(3):463–475.
54. Epstein S (1986) Does aggregation produce spuriously high estimates of behavior stability? *J Pers Soc Psychol* 50(6):1199–1210.
55. Rushton JP, Brainerd CJ, Pressley M (1983) Behavioral development and construct validity: The principle of aggregation. *Psychol Bull* 94(1):18–38.

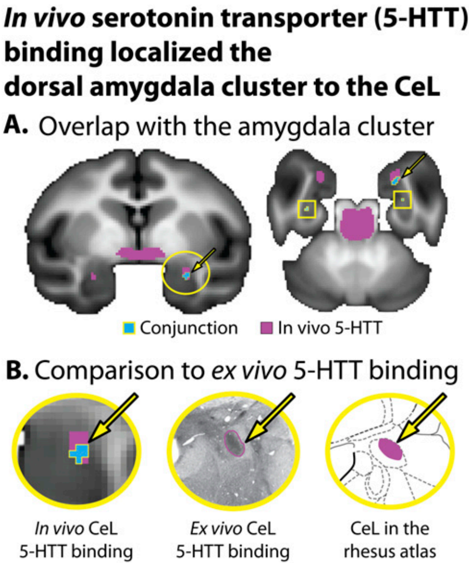

Fig. S1. In vivo serotonin transporter (5-HTT) binding localized the dorsal amygdala cluster to the CeL. High levels of 5-HTT binding are a hallmark of the lateral subdivision of the CeL. (*A*) Overlap between the amygdala cluster from the conjunction analysis (gold arrow; see Fig. 3) and in vivo 5-HTT availability (magenta). High 5-HTT availability was also observed along the midline (substantial innominata and raphe), but not in the anterior hippocampal clusters shown in the axial view (gold boxes). (*B*) Comparison with ex vivo 5-HTT binding. From left to right, magnified coronal views of the overlap shown in *A*, ex vivo 5-HTT binding, and the CeL in the rhesus atlas [adapted with permission from ref. 25, Copyright Elsevier (2009)]. The ex vivo image is a low-power photomicrograph of 5-HTT immunohistochemistry [adapted with permission from ref. 47, Copyright Elsevier (2006)].

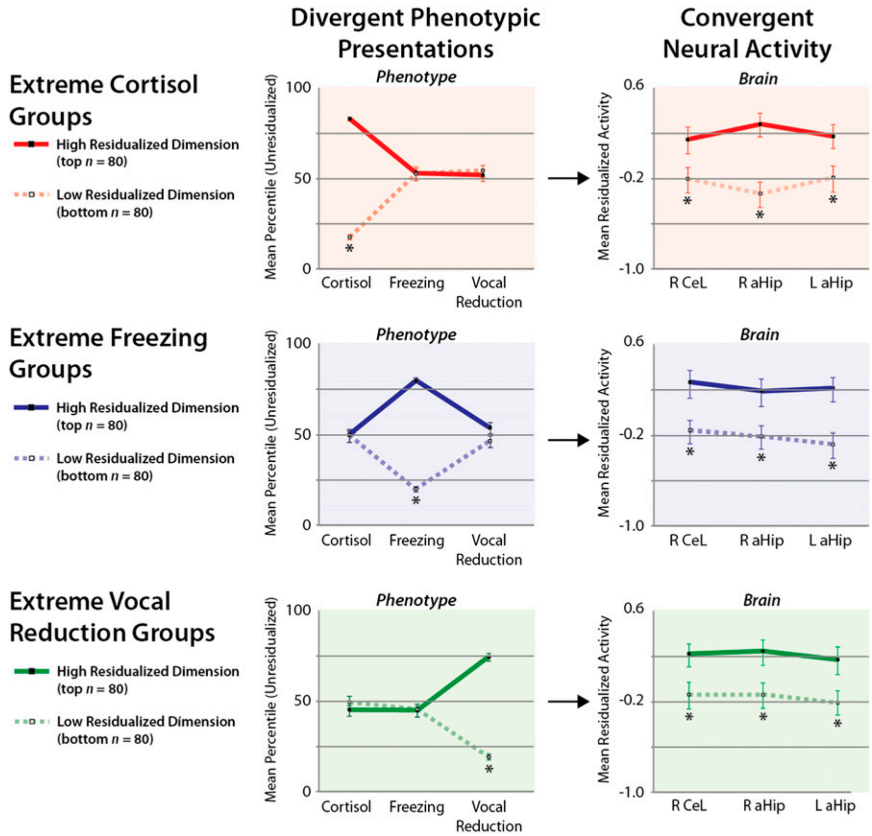

Fig. S2. Implications of the partial correlation analyses illustrated using a tercile split of the three residualized AT dimensions. The conjunction analysis demonstrates a consistent pattern of metabolic activity in the CeL and anterior hippocampus across divergent presentations of the AT phenotype. Divergent phenotypic presentations: To illustrate these effects, we plotted mean phenotype profiles for groups of individuals with high or low levels of each AT dimension. As with the partial correlation analyses, each dimension was residualized to remove variance predicted by the other two. A tercile split was used to identify extreme groups (n = 80 per group) separately for each residualized dimension (*Top* tercile: solid lines; *Bottom* tercile: broken lines). The panels on the left illustrate how this procedure sorts individuals into groups with divergent presentations of AT. Convergent neural activity: To illustrate the consistency of neural activity across divergent presentations, mean neural activity for the extreme groups (± SEM) is shown on the right. Individuals with high levels of cortisol, freezing, or vocal reductions (and intermediate levels of the other two responses on average) evinced greater activity compared with those with low levels. aHip, anterior hippocampus; CeL, lateral division of the central nucleus of the amygdala; L, left; R, right.

Table S1. Cluster descriptive statistics for regions where cerebral metabolism predicts cortisol

Sign of the partial correlation	Cluster	Cluster volume (mm³)	Regions within the cluster	Millimeters from AC In template *x*	*y*	*z*	Cortisol partial correlation *t**	Cortisol vs. freezing *t*†	Cortisol vs. vocal reductions *t*†
Regions where cerebral metabolism significantly predicts cortisol after controlling for variation in freezing and vocal reductions‡									
Negative	Bi visual	3092.04	R V1	2.500	−44.375	1.250	−3.42	NA	NA
			R V2	−9.375	−36.250	10.000	−3.34	NA	NA
			R V2/V3V	15.000	−38.750	−8.750	−4.56	NA	NA
			R V2/V3D	15.625	−33.750	6.250	−3.22	NA	NA
			R V4V	21.250	−26.875	−8.125	−3.43	NA	NA
	L visual	0.49	V1	−15.625	−33.750	6.250	−2.81	NA	NA
	L visual	450.20	V1/V2	−15.625	−33.750	6.250	−2.81	NA	NA
			V3V	−8.125	−43.125	−8.750	−4.69	NA	NA
	L parietal	49.07	PE in the depths of IPS	−10.625	−21.250	13.750	−3.57	NA	NA
	L central	342.29	PE	−18.125	−15.625	16.875	−3.11	NA	NA
			Area 1	−21.250	−5.625	13.125	−3.87	NA	NA
			Area 2	−21.875	−9.375	11.875	−3.47	NA	NA
			Area 4 (F1)	−18.750	−4.375	11.875	−3.77	NA	NA
	R central	1352.05	PE	18.125	−12.500	15.625	−4.68	NA	NA
			Area 3A	18.750	−5.000	8.750	−4.15	NA	NA
			S2	20.625	−5.625	6.250	−4.06	NA	NA
			Area 2	21.250	−11.250	10.625	−3.93	NA	NA
			Area 4 (F1)	19.375	−3.750	16.875	−3.14	NA	NA
			Areas 44/6VR (F5) adjacent to IAR	21.250	4.375	9.375	−3.49	NA	NA
	L motor	1.46	Area 4 (F1)	−10.000	−12.500	21.875	−2.85	NA	NA
	L midcingulate	18.80	Areas p32′/24d′ in the fundus of CgS	−5.625	−2.500	13.750	−3.23	NA	NA
	R OFC	12.70	Areas 11/47	15.000	20.000	6.875	−3.38	NA	NA
Positive	R brainstem	0.73	Brainstem	1.875	−13.125	−10.000	2.81	NA	NA
	L midbrain	177.00	Colliculus	−3.125	−18.750	−2.500	4.12	NA	NA
			Isthmus of the cingulate	−3.125	−18.750	1.250	3.73	NA	NA
	R midbrain	71.53	Colliculus	3.750	−18.750	−3.125	3.77	NA	NA
	Bi thalamus	352.54	L dorsal thalamus	−5.000	−10.625	3.125	4.01	NA	NA
			R dorsal Thalamus	3.750	−8.750	5.000	3.77	NA	NA
	Bi striatum	343.02	L BNST	−2.500	2.500	−0.625	3.07	NA	NA
			L Caudate	−2.500	5.000	2.500	3.25	NA	NA
			L Lat septum	−1.875	3.750	2.500	3.24	NA	NA
			R Lat septum	1.250	3.125	0.625	3.16	NA	NA
			R Caudate	3.750	4.375	3.750	3.34	NA	NA
	L Ant hippocampus‡	1236.33	TF	−18.750	−11.250	−12.500	4.80	NA	NA
			Area 36 (TLR)	−16.250	−7.500	−15.000	4.58	NA	NA
			Ant hippocampus	−13.125	−3.750	−10.000	4.89	NA	NA
	R Ant hippocampus§	65.43	Caudal entorhinal	9.375	−2.500	−13.750	3.23	NA	NA
			Areas 35/36 (TLR)	19.375	−8.125	−15.000	5.50	NA	NA
			Ant hippocampus	−16.875	−6.250	−11.250	5.92	NA	NA
	L post hippocampus	51.27	Post hippocampus	−12.500	−17.500	−4.375	3.73	NA	NA
	R post hippocampus	65.43	Post hippocampus	12.500	−18.125	−3.750	3.75	NA	NA
	L Sup temporal	321.53	PaAL	−28.125	−10.000	1.875	4.76	NA	NA
	R Sup temporal	293.95	TPO	24.375	−11.250	0.000	4.15	NA	NA
			ST2	24.375	2.500	−4.375	3.87	NA	NA
			PaAL	28.750	−6.250	−1.875	3.39	NA	NA
	R claustrum	22.22	Claustrum	12.500	6.875	−3.125	3.24	NA	NA
	R OFC	7.57	Area 13L	12.500	11.875	3.750	3.21	NA	NA
Regions where cerebral metabolism significantly and selectively predicts cortisol									
Negative	R Lat visual	0.24	V2	16.875	−39.375	−8.750	−4.21	−3.02	−2.97
	L Lat visual	8.30	V4D/TEO	−21.250	−23.750	0.000	−3.03	−3.93	−3.58
	R Lat visual	90.58	V4V	20.625	−30.000	−3.125	−2.94	−3.09	−3.24
			V3	20.625	−30.000	1.250	−3.23	−4.06	−3.22
			V4D/TEO	22.500	−24.375	2.500	−3.28	−3.73	−3.76
	R parietal	0.24	Area PE in IPS	18.750	−13.75	15.000	−4.30	−2.97	−3.14
	R mid-insula	34.42	Gustatory Cortex and S2	18.125	−4.375	4.375	−3.41	−5.65	−3.12

Table S1. Cont.

Sign of the partial correlation	Cluster	Cluster volume (mm^3)	Regions within the cluster	Millimeters from AC In template *x*	*y*	*z*	Cortisol partial correlation *t**	Cortisol vs. freezing $t^{\dagger}$	Cortisol vs. vocal reductions $t^{\dagger}$
Positive	R cerebellum	38.33	Paraflocculus	−15.625	−16.875	−10.625	4.23	5.59	3.04
	L parahippocampus	0.24	PHG and isthmus of the cingulate	−10.625	−18.750	−4.375	2.96	4.83	2.97
	R parahippocampus	3.91	PHG and isthmus of the cingulate	12.500	−18.750	−4.375	3.56	2.99	3.02
	L Inf temporal	8.54	Area 36 (TH)	−18.750	−11.250	−12.500	4.79	2.97	4.14
	R Inf temporal	99.12	Area 36 (TH)	16.250	−9.375	−13.750	5.17	3.00	2.98
	L post cingulate	37.35	Area 23	−3.125	−18.750	1.250	3.73	3.20	3.08
	R hippocampus	6.84	Lat Ant hippocampus	16.875	−6.250	−11.250	5.92	3.49	3.29

AC, anterior commissure; Ant, anterior; Bi, bilateral; BNST, bed nucleus of the stria terminalis; CeL, lateral division of the central nucleus of the amygdala; CgS, cingulate sulcus; dlPFC, dorsolateral prefrontal cortex; IAR, inferior arcuate sulcus; Inf, inferior; IPS, intraparietal sulcus; L, left; Lat, lateral; NA, not applicable; OFC, orbitofrontal cortex; PHG, parahippocampal gyrus; Post, posterior; R, right; Sup, superior. White matter clusters are omitted. Regions were labeled using Paxinos et al. (25), freely available at http://scalablebrainatlas.incf.org/main/coronal3d.php?template=PHT00&.

*Robust regression controlling for variation in mean-centered age, sex, gray matter probability, standardized freezing duration, and standardized vocal reductions (whole-brain FDR $q < 0.05$).

†Williams T2 test for the difference in dependent correlations (whole-brain FDR $q < 0.05$).

‡Cluster contains the left anterior hippocampal cluster identified as a shared substrate (see Table S4).

§Cluster contains the right anterior hippocampal and dorsal amygdala (CeL) clusters identified as shared substrates (Table S4).

Table S2. Cluster descriptive statistics for regions where cerebral metabolism predicts freezing

Sign of the partial correlation	Cluster	Cluster volume (mm^3)	Freezing: Regions within the cluster	Millimeters from AC in template *x*	*y*	*z*	Freezing partial correlation *t**	Freezing vs. cortisol $t^{\dagger}$	Freezing vs. vocal reductions $t^{\dagger}$
Regions where cerebral metabolism significantly predicts freezing after controlling for variation in cortisol and vocal reductions									
Negative	Bi hemispheres	17882.32	L Ventral parafloccus	−15.625	−18.125	−11.250	−4.44	NA	NA
			R ventral parafloccus	15.000	−20.000	−10.625	−3.84	NA	NA
			R CB5 and ventral parafloccus	15.625	−26.250	−8.750	−5.16	NA	NA
			L CB5	−1.250	−23.750	−5.000	−4.70	NA	NA
			R CB5	2.500	−23.750	−3.750	−4.61	NA	NA
			L V2/V1	−9.375	−27.500	−2.500	−8.19	NA	NA
			R V1	10.625	−25.000	2.500	−6.20	NA	NA
			R V2	5.625	−30.625	0.000	−7.42	NA	NA
			R MST	13.125	−24.375	12.500	−4.84	NA	NA
			R MST and TPOC	15.000	−24.375	8.125	−5.68	NA	NA
			L PO and V3D in the fundus of POS	−6.875	−33.750	6.250	−4.49	NA	NA
			L V4	−18.125	−25.625	−7.500	−4.12	NA	NA
			L MSTV and MT (V5)	−15.000	−24.375	8.750	−4.56	NA	NA
			L PEC and PGM	−3.125	−31.250	13.750	−4.36	NA	NA
			L PE (MIP) in the depths of IPS	−10.625	−23.125	16.875	−7.98	NA	NA
			L PO (LIPE) in the depths of IPS	−9.375	−25.000	13.125	−5.02	NA	NA
			R PO (LIPE/LIPI) in the depths of IPS	6.875	−26.250	13.750	−5.07	NA	NA
			R areas 6/32′ (gyral) and 4 (F1)	0.000	−4.375	17.500	−4.08	NA	NA
			L dorsal area 4 (F1)	−6.250	−11.250	22.500	−6.39	NA	NA
			R dorsal area 4 (F1)	3.750	−11.875	21.875	−6.30	NA	NA
			R Lat area 4 (F1)	13.750	−8.750	17.500	−6.24	NA	NA
			L area 8D in the depths of SAR	−11.875	3.750	11.250	−3.79	NA	NA
			R area 8D in the depths of SAR	10.000	4.375	14.375	−3.70	NA	NA
			R area 6DR (F7)	10.625	8.125	16.875	−3.46	NA	NA
Positive	L Lat visual	1336.91	Lat V2	−28.125	−27.500	0.000	5.46	NA	NA
			TEO	−28.750	−20.625	0.625	4.74	NA	NA
			TEM and TE3	−28.750	−13.750	−1.875	3.57	NA	NA
	L midbrain	0.49	Midbrain	−2.500	−5.625	−6.250	2.80	NA	NA

Table S2. Cont.

Sign of the partial correlation	Cluster	Cluster volume (mm^3)	Freezing: Regions within the cluster	Millimeters from AC in template			Freezing partial correlation t*	Freezing vs. cortisol t†	Freezing vs. vocal reductions t†
				x	y	z			
	R midbrain	4.64	Reticular formation	5.625	−9.375	−6.250	2.88	NA	NA
	L hemisphere‡	6728.52	Lat nucl. of the amygdala	−13.125	1.875	−10.000	3.33	NA	NA
			Piriform and claustrum	−12.500	3.750	−6.250	3.57	NA	NA
			PFG and PFOp	−25.000	−11.875	10.625	4.24	NA	NA
			TE	−23.125	0.000	−14.375	3.20	NA	NA
			TPPro	−20.000	6.875	−9.375	4.12	NA	NA
			Area 38 (TLR)	−13.125	7.500	−15.625	3.33	NA	NA
			S2	−23.125	−3.750	3.125	6.86	NA	NA
			Gustatory cortex and AI	−19.375	6.250	1.250	5.84	NA	NA
			Area 4 (F1)	−27.500	−1.250	8.125	3.71	NA	NA
			Area 6VR (F5)	−23.125	7.500	6.250	5.04	NA	NA
			Area 47L	−23.125	13.125	−0.625	4.42	NA	NA
			Area 47O	−18.125	10.625	0.625	5.45	NA	NA
	R Hemisphere §	6176.03	Lat V2	26.250	−26.875	−1.875	5.16	NA	NA
			Ce and ventral putamen	13.125	−4.375	−6.875	4.37	NA	NA
			GI, ProKM, and Claustrum	18.125	−6.250	−3.750	4.87	NA	NA
			Area 2	24.375	−11.875	10.625	3.84	NA	NA
			TE3 and TEO	28.750	−17.500	−1.250	3.75	NA	NA
			TPO and TAa	22.500	0.625	−9.375	5.67	NA	NA
			Areas S2 and 2/1	23.750	3.125	−1.250	7.06	NA	NA
			Gustatory cortex	21.250	5.625	0.000	6.97	NA	NA
			Area 47	15.000	20.000	6.875	3.43	NA	NA
	L temporal	0.98	TE3	−26.250	−8.750	−11.250	2.83	NA	NA
	R temporal	3.91	TE3	25.625	−10.000	−12.500	3.05	NA	NA
	R temporal pole	66.16	Areas 36 (TLR) and TPPro	15.000	7.500	−16.875	3.43	NA	NA
	L vmPFC	197.51	Area 14M	−0.625	25.000	1.875	3.00	NA	NA
	R dlPFC	39.55	Area 8B	5.625	15.625	16.250	2.89	NA	NA
Regions where cerebral metabolism significantly and selectively predicts freezing									
Negative	Bi mesial visual and cerebellum	1284.18	L V2	−9.375	−27.500	−2.500	−8.19	−4.07	−4.77
			Bi CB4/5	−1.250	−23.750	−5.000	−4.70	−3.73	−3.32
			R V2	5.625	−30.625	0.000	−7.42	−2.96	−4.30
			R V1	10.625	−25.000	2.500	−6.20	−4.40	−5.13
			R SCL	15.625	−26.250	−8.750	−5.16	−3.03	−3.68
	R dorsal STS	0.98	MT (V5), MSTV, MSTD, and TPOC	15.625	−24.375	8.125	−5.66	−3.07	−2.95
	L motor	81.79	Dorsomesial area 4 (F1)	−6.250	−11.250	22.500	−6.39	−3.87	−5.66
	L motor	101.81	Lat area 4 (F1) adjacent to CS	−13.125	−6.875	19.375	−5.66	−4.48	−4.75
			Area 6DC (F2)	−12.500	1.250	18.125	−5.48	−4.48	−3.44
	R motor	280.52	Dorsomesial area 4 (F1)	3.750	−11.875	21.875	−6.30	−4.16	−6.36
			Area 4 (F1) along SPCD	9.375	−7.500	20.625	−6.24	−3.47	−5.25
			Lat area 4 (F1) adjacent to CS	13.750	−8.750	17.500	−6.24	−3.59	−5.19
	L FEF	24.17	Areas 6DR (F7) and 8AD/B in the fundus of SAR	−11.875	3.750	11.250	−3.79	−3.23	−3.83
	R FEF	0.24	Area 6DC (F2) in the posterior-dorsal bank of SAR	15.000	0.625	15.625	−4.14	−3.00	−3.01
Positive	L Lat visual	92.77	V1	−28.125	−27.500	0.000	5.46	4.79	3.49
	R Lat visual	118.90	V1	26.250	−26.875	−1.875	5.16	5.11	3.33
	L temporal	1.22	Area TEO	−28.750	−20.625	0.625	4.74	3.72	2.98
	R temporal	1.22	Area TPO	21.250	2.500	−9.375	5.22	2.96	4.12
	L insula/OFC	1891.60	Area PFx	−25.000	−11.875	10.625	4.24	4.72	3.66
			GI, claustrum, and putamen	−17.500	−6.875	−3.750	5.74	3.32	4.49

Table S2. Cont.

Sign of the partial correlation	Cluster	Cluster volume (mm³)	Freezing: Regions within the cluster	Millimeters from AC in template			Freezing partial correlation *t**	Freezing vs. cortisol *t*†	Freezing vs. vocal reductions *t*†
				x	*y*	*z*			
			S2	−24.375	2.500	1.875	6.59	5.53	5.68
			AI and S2	−19.375	6.250	1.250	5.84	4.69	4.81
			Dorsal Area 6VR (F5)	−23.125	7.500	6.250	5.04	4.89	4.23
			Areas 44, 47O, and ProM	−18.125	10.625	0.625	5.45	3.51	4.91
			Area 47L	−23.125	13.125	−0.625	4.42	4.45	4.32
	R insula/OFC	1492.43	Area PFx	24.375	−11.875	10.625	3.84	5.33	2.96
			GI, Claustrum, and Putamen	16.875	−9.375	−0.625	4.55	2.99	3.58
			S2	21.250	−4.375	3.125	6.54	6.91	5.11
			Ventral Area 2/1	23.750	3.125	−1.250	7.06	4.38	7.06
			Gustatory Cortex	21.250	5.625	0.000	6.97	4.77	6.46
			Area 47L	24.375	11.250	1.875	5.16	4.55	4.80
	L OFC	11.96	Area 47	−15.625	19.375	6.875	3.85	3.77	3.38
	R OFC	25.15	Area 47	15.000	20.000	6.875	3.43	4.93	3.51

AC, anterior commissure; AI, anterior insula; Bi, bilateral; CeL, lateral division of the central nucleus of the amygdala; CS, central sulcus; dlPFC, dorsolateral prefrontal cortex; FEF, frontal eye field; GI, granular insula; IAR, inferior arcuate sulcus; IPS, intraparietal cortex; L, left; Lat, lateral; NA, not applicable; Nucl, nucleus; OFC, orbitofrontal cortex; POS, parieto-occipital sulcus; R, right; SAR, superior arcuate sulcus; SCL, simple cerebellar lobule; SPSD, superior precentral dimple; STS, superior temporal sulcus; vmPFC, ventromedial prefrontal cortex. White matter clusters are omitted. Regions were labeled using Paxinos et al. (25), freely available at http://scalablebrainatlas.incf.org/main/coronal3d.php?template=PHT00&.

*Robust regression controlling for variation in mean-centered age, sex, gray matter probability, standardized plasma cortisol, and standardized vocal reductions (whole-brain FDR $q < 0.05$).

†Williams T2 test for the difference in dependent correlations (whole-brain FDR $q < 0.05$).

‡Cluster contains the left anterior hippocampal cluster identified as a shared substrate(see Table S4).

§Cluster contains the right anterior hippocampal and dorsal amygdala (CeL) clusters identified as shared substrates (see Table S4).

Table S3. Cluster descriptive statistics for regions where cerebral metabolism predicts vocal reductions

Sign of the partial correlation	Cluster	Cluster volume (mm³)	Vocal reductions: Regions within the cluster	mm from AC in template			Vocal reductions partial correlation *t**	Vocal reductions vs. cortisol *t*†	Vocal reductions vs. freezing *t*†
				x	*y*	*z*			
Regions where cerebral metabolism significantly predicts vocal reductions after controlling for variation in cortisol and freezing									
Negative	R visual	2.44	V2	6.875	−21.875	−2.500	−2.90	NA	NA
	Bi visual	480.47	L V2	−7.500	−21.250	−1.875	−3.79	NA	NA
			L PGM	−2.500	−33.750	3.125	−2.97	NA	NA
			R PGM	1.875	−28.125	5.000	−3.15	NA	NA
			L area 23 and PGM	−1.875	−22.500	5.000	−4.42	NA	NA
	R dorsal parietal	494.63	DP	10.000	−31.875	17.500	−4.34	NA	NA
	R Lat parietal	31.49	PG	20.000	−23.750	11.250	−3.50	NA	NA
	L OFC/vlPFC	39.55	ProM	−25.000	6.250	−0.625	−3.30	NA	NA
	R OFC/vlPFC	83.25	ProM	23.750	8.750	−2.500	−3.86	NA	NA
Positive	R PAG	181.88	PAG	0.625	−15.625	−2.500	3.79	NA	NA
	Bi thalamus	594.24	L dorsal thalamus	−1.250	−3.750	4.375	4.21	NA	NA
			R dorsal thalamus	0.625	−3.750	4.375	4.18	NA	NA
			L ventral Ant thalamus	3.125	−3.125	0.000	4.50	NA	NA
	L hippocampus‡	63.23	Ant hippocampus	−15.625	−11.875	−7.500	3.42	NA	NA
	R hippocampus§	34.67	Ant hippocampus	16.250	−11.250	−10.000	3.48	NA	NA
	R amygdala¶	137.45	Ce	10.625	−1.250	−8.125	3.36	NA	NA
Regions where cerebral metabolism significantly and selectively predicts Vocal reductions									
Negative	R Parietal	0.24	DP	10.625	−33.125	17.500	−4.01	−3.07	−2.95
	R vlPFC	5.62	ProM and ST2	23.125	5.000	−3.125	−3.15	−3.63	−6.91

AC, anterior commissure; Ant, anterior; Bi, bilateral; Ce, central nucleus of the amygdala; CeL, lateral division of the central nucleus of the amygdala; Lat, lateral; L:,left; OFC, orbitofrontal cortex; PAG, periaqueductal gray; R, right; vlPFC, ventrolateral prefrontal cortex. White matter clusters are omitted. Regions were labeled using Paxinos et al. (25), freely available at http://scalablebrainatlas.incf.org/main/coronal3d.php?template=PHT00&.

*Robust regression controlling for variation in mean-centered age, sex, gray matter probability, standardized cortisol, and standardized freezing duration (whole-brain FDR $q < 0.05$).

†Williams T2 test for the difference in dependent correlations (whole-brain FDR $q = 0.05$).

‡Cluster contains the left anterior hippocampal cluster identified as a shared substrate (Table S4).

§Cluster contains the right anterior hippocampal cluster identified as a shared substrate (Table S4).

¶Cluster contains the right dorsal amygdala (CeL) cluster identified as a shared substrate (Table S4).

Table S4. Cluster descriptive statistics for regions where cerebral metabolism predicts the unique variance in standardized plasma cortisol levels, freezing, and vocal reductions

Cluster	Cluster volume (mm^3)	Millimeters from AC in template			Three-way conjunction of partial correlations*
		x	*y*	*z*	Robust minimum *t*[†]
R dorsal amygdala[‡]	4.394	11.875	−1.250	−9.375	2.96
R anterior hippocampus	0.244	14.375	−6.875	−9.375	2.81
L anterior hippocampus	0.732	−15.625	−10.000	−9.375	2.87

*Robust regression controlling for variation in mean-centered age, sex, and voxelwise GM probability.
[†]Minimum across the three thresholded partial correlation maps (whole-brain FDR $q < 0.05$).
[‡]As detailed in *SI Methods*, hemispheric asymmetry analyses for the right dorsal amygdala cluster were not significant.

Table S5. Descriptive statistics for cluster mediation analyses

Candidate mediating region[‡]	AT dimension	Common substrates[¶]	Mediation test		Effect sizes for mediation paths (regressions): Common substrate → AT dimension	Common substrate → Candidate mediator	Candidate mediator → AT dimension	Specificity analyses: Control mediating region: M1*		Lat Ant hippo[†]		Control AT dimension: Freezing		Cortisol	
			Tt	*P*[§]	*t*[‖]	*t*[‖]	*t*[‖]	*t*[**]	*P*[§]	*t*[**]	*P*[§]	*t*[††]	*P*[§]	*t*[††]	*P*[§]
Lat Ant hippo[†]	Cortisol	L Ant hippo	4.09	<0.005	3.09	11.00	5.40	−0.05	NS	—	—	−0.86	NS	—	—
		R Ant hippo	2.99	<0.005	4.53	16.40	5.40	−0.46	NS	—	—	−1.57	NS	—	—
		R CeL	4.36	<0.005	3.07	8.69	5.40	−0.15	NS	—	—	−0.56	NS	—	—
M1*	Freezing	L Ant hippo	5.19	<0.005	2.55	−4.41	−5.54	—	—	−0.86	NS	—	—	−0.05	NS
		R Ant hippo	5.00	<0.005	3.01	−4.21	−5.54	—	—	−1.57	NS	—	—	−0.46	NS
		R CeL	4.73	<0.005	3.25	−4.60	−5.54	—	—	−0.56	NS	—	—	−0.15	NS
vlPFC[‡‡]	Vocal reductions	L Ant hippo	−3.63	NS[¶¶]	2.79	1.03	−3.13	—	—	—	—	—	—	—	—
		R Ant hippo	−3.17	NS[¶¶]	2.55	2.08	−3.13	—	—	—	—	—	—	—	—
		R CeL	−3.95	NS[¶¶]	2.89	3.83	−3.13	—	—	—	—	—	—	—	—

Ant, anterior; AT, anxious temperament; CeL, the lateral division of the central nucleus of the amygdala; Hippo, hippocampus; L, left hemisphere; Lat, lateral; M1, primary motor cortex (area 4); NS, nonsignificant ($P > 0.05$, one-tailed, Sidak-corrected for nine tests); R, right hemisphere; vlPFC, ventrolateral prefrontal cortex. Regions were labeled using Paxinos et al. (25), freely available at http://scalablebrainatlas.incf.org/main/coronal3d.php?template=PHT00&.
*The dorsomesial motor region (area 4) that was selective to freezing (Table S2).
[†]The lateral anterior hippocampal region that was selective to cortisol (Table S1).
[‡]Hypothesis testing focused on whether selective regions mediated the association between each of the three core (common) regions and the three dimensions of the AT phenotype.
[¶]The three regions detailed in Table S4.
[§]Uncorrected *P*.
[‖]OLS regression controlling for variation in mean-centered age, sex, GM probability, and the two nontarget AT dimensions (i.e., a partial correlation analysis). Significant results for the corresponding whole-brain robust regressions (FDR $q < 0.05$) are detailed in Tables S1–S4.
**T-statistic for the mediation test using a control region (e.g., testing whether the lateral anterior hippocampal region that was selective to cortisol mediates the association between CeL and freezing).
[††]T-statistic for the mediation test using a control dimension of AT (e.g., testing whether M1 mediates the association between Ce and cortisol).
[‡‡]The vlPFC region that was selective to vocal reductions (Table S3).
[¶¶]This region displayed a suppressive relationship; the amount of variance in vocal reductions that was predicted by each one of the shared substrates was increased rather than decreased after accounting for the influence of the candidate mediator (vlPFC).